ISSN: 2634 - 8845

Journal of Earth and Environmental Science Research

Research Article

Open Access

Deformation Monitoring and Analysis of Mountainous Cut and Fill Airport Construction Considering Topographic and Geomorphological Features: A Case Study of Weining Caohai Airport

Jun Lu[1], Dao Qin Zhou[1], Bing Xu[2]*, Jie Li[2], Kexin Chen[2], Guoliang Zhao[3], Dong Lei Ma[3] and Tao Xie[1]

[1]Third Surveying and Mapping Institute of Guizhou Province, Guiyang, 500004, China

[2]School of Geoscience and Info-Physics, Central South University, Changsha 410083, Hunan, China

[3]Beijing Geoway Info-Tech Co., Ltd., Beijing 100043, China

ABSTRACT

The rapid expansion of aviation infrastructure has intensified requirements for mountainous airport construction, where engineering activities involving extensive fill embankments and deep excavations induce significant surface deformation that jeopardizes operational safety. Conventional geodetic techniques (e.g., GPS networks and leveling surveys) present limitations in spatiotemporal resolution for large-area, high-precision deformation monitoring requirements. This study investigates surface displacement at Guizhou Weining Caohai Airport through an enhanced time-series InSAR methodology incorporating topographic and geomorphological characteristics. We employ multi-source remote sensing data including ascending/descending orbit SAR acquisitions from China's Land Exploration Satellite-1 (LT-1) mission (2023-2025) and Sentinel-2 optical imagery. Our methodological innovations include: 1) Optimized homogeneous pixel identification criteria through integration of a priori topographic parameters (slope gradient, aspect orientation) and land cover classification; 2) Enhanced phase reliability through weighted confidence interval estimation coupled with maximum likelihood phase optimization, significantly improving measurement accuracy in complex terrain; 3) Development of a slope-aspect-constrained 2D deformation decomposition model leveraging multi-orbit SAR geometries to resolve vertical and characteristic horizontal displacement components. The experimental results validate the technical efficacy of the improved InSAR framework for mountainous airport monitoring, establishing a scientific foundation for infrastructure safety management and geohazard mitigation strategies.

***Corresponding author**

Bing Xu, School of Geoscience and Info-Physics, Central South University, Changsha 410083, Hunan, China.

Received: November 07, 2025; **Accepted:** November 10, 2025; **Published:** November 21, 2025

Keywords: Mountain Airports, Time Series InSAR, Terrain Features, Deformation Decomposition, Weining Caohai Airport

Introduction

As the global aviation industry develops and demand for civil aviation transport continues to grow, airlines and airports are increasing their infrastructure development, especially in geographically complex areas, such as the mountainous regions in the west of the country, where airport construction has become an important way to solve transport problems. Mountain airports not only connect remote areas and promote economic development, but also improve accessibility. However, airport construction in mountainous areas faces greater challenges. Flat areas have a natural advantage in airport construction. But even in flat areas, airport runways and facilities can suffer from settlement, cracks, and collapse due to natural and man-made factors. For this reason, scholars have conducted deformation monitoring studies on Beijing Capital International Airport, Shanghai Pudong International Airport, and Hong Kong Chek Lap Kok International Airport [1-3]. Compared with flat areas, mountainous areas have complex terrain, and airport construction often requires deep excavation and high fill, and there are often weak soil layers at the bottom of high fill foundations, which makes the project difficult. Airports like Jiuzhai Huanglong Airport, Kangding Airport, Panzhihua Airport and Liupanshui Airport face these problems [4-7]. If settlement deformation occurs in critical areas such as runways, it can threaten flight safety and normal airport operations. Therefore, effective monitoring of post-industrial deformation of mountain airports to ensure the stability of facilities and flight safety is a key issue in airport construction.

Traditional monitoring methods such as GPS, levelling and total stations are highly accurate, but have limited temporal and spatial resolution and cannot accurately reflect deformation. Optical satellites solve the problem of resolution, but are susceptible to weather and insensitive to small deformations. Interferometric Synthetic Aperture Radar (InSAR) technique is very sensitive to small deformations through phase observation, which provides a new solution for post-industrial deformation monitoring at airports. In addition, the combination of time-series InSAR technique and the theory of characteristic deformation decomposition will further improve the accuracy and reliability of post-work deformation monitoring in mountainous airports. Considering the influence of topographic relief on deformation, deformation decomposition based on mountainous terrain features can not only identify the spatial distribution characteristics of deformation in a finer way, but also provide more targeted analysis and processing methods for different types of deformation. The time series InSAR technique can more accurately reveal the specific process of soil deformation during the construction of mountainous airports, and thus provide a more scientific guarantee for the long-term stability of airport facilities. The Differential Synthetic Aperture Radar Interferometry (D-InSAR) is a method to monitor the surface deformation by using SAR (synthetic aperture radar) technique. It reveals small displacements of the ground surface by comparing SAR images at different points in time, and is widely used in the fields of geological disasters and urban settlement. Since the D-InSAR technique was proposed and applied to surface deformation monitoring in 1989, a variety of InSAR techniques have been developed and applied to the field of surface deformation monitoring [8-11]. However, D-InSAR is affected by spatiotemporal incoherence and atmospheric delay, and thus has certain limitations. To overcome these problems, time-series InSAR techniques (PS-InSAR and SBAS-InSAR) have emerged, which are capable of monitoring surface deformation with high accuracy through multi-temporal image analysis, and are particularly suitable for long-term and large-scale deformation monitoring, such as earthquakes, landslides, and subsidence. Typical time-series InSAR techniques include PS-InSAR and SBAS-InSAR [12,13]. Both of them have wide applications in deformation monitoring of airports.

Wu Yibin used the time series InSAR technique to obtain the time deformation sequence of Xiamen new airport reclamation area, and analyzed the characteristics of the deformation field and the causes of subsidence [14]. Mei Huihui and others used SBAS-InSAR and PS-InSAR techniques to extract the deformation information of the runway of Yanshan Airport, Wenshan, Yunnan, respectively, and cross-validated the results obtained by the two methods to analyses the temporal and spatial characteristics of the surface deformation of the airport runway and the reasons for the occurrence of deformation [15]. Luo Xianbin inverted the settlement information of two reclaimed airports built in different periods, Shanghai Pudong International Airport and Hong Kong International Airport, based on the time-series InSAR technique, and constructed a long short-term memory (LSTM) network settlement prediction model, and selected the two reclaimed airports' settlement zones for prediction and analysis. Valerio Gagliardi used time-series InSAR to predict the settlement of the runway of Rome Fiumicino Airport, which is located on the south side of the airport [16,17]. deformation monitoring of the runway area of Rome Fiumicino Airport, which identified localized runway settlements and optimized the runway maintenance programmed.

In summary, the construction of airports in mountainous areas is faced with complex terrain and geomorphological features, and post-construction deformation problems due to the extensive cut-and-fill construction methods are a major challenge affecting the quality of the work and flight safety. The deformation of cut-and-fill airports in mountainous areas is more pronounced than that of airports in flat areas, and the monitoring of deformation is more challenging. In this paper, we use the time-series InSAR technique, which takes into account the topographic and geomorphological features, to monitor the surface deformation during the cut-and-fill construction of airports in mountainous areas, and combine the high-precision deformation data with the analysis of the deformation patterns of different geomorphological features under the complex terrain and geological conditions in mountainous areas, so as to ensure the stability and safety of the airfield facilities, and to provide scientific support for the early warning and prevention of the subsidence of the airports and the surrounding geologic hazards.

Methodology

DS-InSAR Deformation Monitoring Methodology Taking into Account Topographic and Geomorphological Features

DS-InSAR techniques include homogeneous point identification of distributed targets and DS point phase optimization studies. Homogeneous point identification refers to discriminate whether two image elements within a certain spatial range in a SAR image dataset belong to the same feature. The main principle of the algorithm is to extract the intensity information of the same image element in the time dimension and measure the similarity of the two samples, so as to judge whether they are homogeneous points.

Based on the assumption that the radar signal of any image element in the SAR image dataset obeys the complex Gaussian distribution and the mean value of its amplitude in the time dimension obeys the Rayleigh distribution, the traditional hypothesis testing method is converted to confidence interval estimation, and a simple logical calculation is performed to judge whether two image elements obey the same functional distribution, so as to achieve the purpose of image homogeneous point identification. For a DS point p to be estimated, its confidence interval estimation can be written as:

$$P\left\{\mu(p) - z_{1-\frac{\alpha}{2}} \cdot 0.52 \cdot \frac{\mu(p)}{\sqrt{N}} < \bar{A}(p) < \mu(p) + z_{1-\frac{\alpha}{2}} \cdot 0.52 \cdot \frac{\mu(p)}{\sqrt{N}}\right\} = 1 - \alpha \tag{1}$$

If $\bar{A}(p)$ is taken as the truth value of the mean pixel intensity value, the above formula is a definite interval, and when the confidence level α is given, it can be judged whether the image to be estimated and the target image are homogeneous by calculating whether the mean intensity value in the time dimension of the image to be estimated falls into the interval corresponding to the target image.

The complex terrain of mountain airports, including plateaus, hills and valleys, poses a challenge to DS-InSAR technique. The undulating terrain can easily lead to shadowing and masking of SAR images, which affects the interference quality. Complex climate exacerbates the atmospheric delay error; drastic terrain changes may aggravate the incoherence phenomenon. Relying only on the intensity information of SAR images and adopting a single threshold statistical test to select homogeneous pixels not only easily leads to the participation of non-similar pixels in the test, which increases the computational burden, but also increases the probability that the non-similar pixels will be misclassified as homogeneous pixels, which leads to the unreliable results of the subsequent solving, and it is difficult to effectively monitor and analyses the subsidence in the study area. Therefore, this paper introduces external surface feature data such as slope, aspect and feature cover type to optimize the point selection criterion and algorithm, to more accurately identify and different scattering characteristics of the image elements, and to effectively overcome the limitations of the complex surface environment in mountainous airports, so as to improve the accuracy of the time-series InSAR solution results. The algorithm flow is shown in figure 1.

Feature cover types are available through external data products, and slope and aspect can be calculated from DEM data using the following equations:

$$Slope = tan^{-1}\left(\sqrt{\left(\frac{dz}{dx}\right)^2 + \left(\frac{dz}{dy}\right)^2}\right) \tag{2}$$

$$Aspect = tan2^{-1}\left(\frac{dz}{dy}, -\frac{dz}{dx}\right) \tag{3}$$

In the formula, *dz*/*dx* denotes the rate of change in the horizontal direction from the central image element, *dz*/*dy* denotes the rate of change in the vertical direction from the central image element, $\tan^{-1}$ is the inverse tangent function, and $\tan2^{-1}$ is the four-quadrant inverse tangent function. The slope Slope ranges from 0 to 90° and the Aspect ranges from 0 to 360°.

For each image p, a weighting factor is determined based on the properties of its slope, aspect and feature cover type. The feature cover type weight factor W_c can be determined based on a priori knowledge, and the scattering stability and sensitivity to deformation changes of the image elements of different feature cover types will be different, for example, in the region of vegetation cover, as the scattering characteristics of vegetation are easily affected by the season or the growth cycle, its stability is low, and the algorithm assigns the weight factor of this region is relatively small (0.3-0.5), in the region of a water body, its scattering characteristics are stable and external factors interfere less with them, the algorithm assigns a larger weight factor (0.7~0.9) to this region. The slope and aspect weight factors can be determined based on statistical analysis to reflect the degree of influence of different surface features on the SAR backscattering characteristics, and within the window size given by the algorithm, if the difference between the slope and aspect of the remaining image elements within the window and the central image element p exceeds a certain threshold, it will be assumed that the difference between the topographic undulation characteristics of that image element and the central image element p is large, and the algorithm will reduce the weight factor of that image element, specifically:

When the slope difference ΔS≤15°, the weighting factor W_s is set to a larger value (0.8), which indicates that the difference in terrain relief between the two image elements is small and the scattering characteristics are less affected by the slope.

When 15°≤ΔS≤30°, the weighting factor W_s is linearly decreasing and is calculated by the following equation:

$$W_s=0.8-0.053*(\Delta S-15°) \tag{4}$$

When the slope difference ΔS>30^°, the weighting factor W_s is set to a smaller value (0.2), which indicates that the difference in terrain relief between the two image elements is obvious, and the scattering characteristics are more affected by the slope.

When the slope difference ΔA≤60°, the weighting factor W_a is set to a larger value (0.8), which indicates that the slope difference between the two image elements is smaller and the scattering characteristics are less affected.

When 60°≤ΔA≤120°, the weighting factor W_a is linearly decreasing and is calculated by the following equation:

$$W_a=0.8-0.0167*(\Delta A-60°) \tag{5}$$

With the addition of weighting factors, the sample means become weighted averages, i.e., each sample intensity value is multiplied by the corresponding weighting factor and divided by the sum of all weighting factors. Similarly, the sample variance needs to be weighted, and the weighted variance takes into account the weight of each sample to reflect the contribution of different surface features to the scattering variability. Assuming that the distribution of the sample means is close to normal, the interval estimates for a confidence level of 1-α can be expressed as:

$$CI = \bar{\mu}(p) \pm z_{1-\frac{\alpha}{2}} * \frac{\bar{s}(p)}{\sqrt{N}} \tag{6}$$

Where *CI* is the confidence interval, $\bar{\mu}(p)$ is the weighted sample mean, $\bar{s}(p)$ is the weighted sample variance, N is the number of samples, and $z_{1-\alpha/2}$ denotes the1-α/2 quantile of the standard normal distribution.

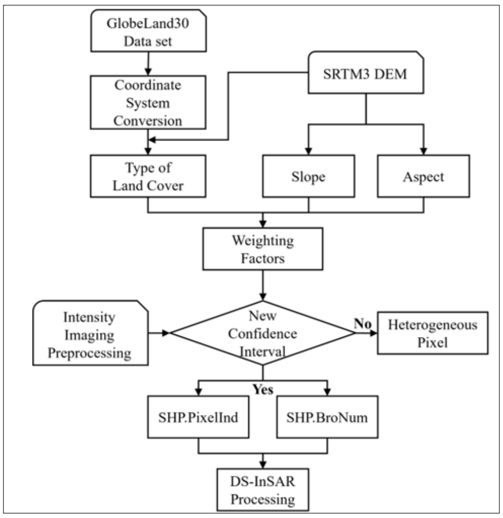

Figure 1: Flowchart of Point Selection Algorithm

The main component of phase optimization is the phase estimation of the equivalent single-master image. The goal of phase estimation for equivalent single-master images is to estimate the phase time series equivalent to a single-master interferogram stack from the phase difference in the multi-master interferogram stack for each detected DS pixel, using maximum likelihood estimation for the conversion process of equivalent single-master images. Maximum likelihood estimation maximizes the multivariate joint probability distribution of the SLC values of the homogeneous regions used for multi-viewing. Assuming that the time-series image element complex values of homogeneous points satisfy the multivariate Gaussian, distribution and are distributed independently of each other among the homogeneous points, the joint probability density function of the image element homogeneous points can be expressed as:

$$f_{d_k}(d_k|\Psi) = c \cdot exp(-d_k^* \Psi \Upsilon^{-1} \Psi^* d_k) \tag{7}$$

Its objective function can be expressed as:

$$\hat{b}_{ML} = \arg\max_b Re(sum(W_{ML} exp^{\circ}(j(y - Bb)))) \tag{8}$$

Expanding it, the objective function can be optimized as follows: expanding it, the objective function can be optimized as follows:

$$\hat{b}_{ML} = \arg\max_b sum(W_{ML} \cos(j(y - Bb))) \tag{9}$$

When the above formula reaches its maximum value, then b^_ML is the optimal solution of the differential phase vector of single primary image obtained by the maximum likelihood estimation method.

Through the above improvement measures, DS-InSAR technique can better adapt to the complex terrain and geomorphology environment, improve the accuracy of deformation monitoring, and provide scientific basis for the safe operation of airports.

A Two-Dimensional Feature Deformation Decomposition Method that Takes into Account Terrain Features

Weining Caohai Airport is a dug-and-filled airport in mountainous areas, and its runway is orientated in a north-south direction, and the deformation of runway slopes mostly occurs in the east-west direction, while the InSAR technique is more sensitive to deformation in the east-west direction, so the time-sequence InSAR technique is suitable for deformation in this study area. The terrain in mountainous areas has large undulations, and single-orbit satellite monitoring will have overlapped and shadowing phenomena, resulting in part of the monitoring area is not obvious. Therefore, the two-dimensional deformation field of the airport area is constructed by combining the results of InSAR time-series deformation monitoring in the elevation orbit, so as to obtain more detailed deformation results in the study area with less data.

The time series InSAR technique is used to obtain the deformation monitoring results of the lift track. The north-south deformation component is ignored, and the deformation information along the east-west and vertical directions is obtained. The LOS deformation of the lifting rail is decomposed as follows:

$$d_{los1} = d_u \times \cos\theta_1 - d_e \times \sin\theta_1 \times \sin\left(\alpha_1 - \frac{3}{2}\pi\right) \tag{11}$$

Therefore, it is possible to use the lift rail data and the results of the deformation in the vertical and east-west directions can be obtained, written in matrix form:

$$\begin{bmatrix} d_{los1} \\ d_{los2} \end{bmatrix} = \begin{bmatrix} \sin\left(\alpha_1 - \frac{3}{2}\pi\right)\sin\theta_1 & \cos\theta_1 \\ \sin\left(\alpha_2 - \frac{3}{2}\pi\right)\sin\theta_2 & \cos\theta_2 \end{bmatrix} \times \begin{bmatrix} d_e \\ d_u \end{bmatrix} \tag{12}$$

When multi-temporal LOS data are available, the two-dimensional deformation sequence decomposition function models along the vertical and east-west directions can be established, and the two-dimensional time series deformation information along the east-west and vertical directions can be computed by iterative weighted least-squares solving.

However, the construction of mountain airports carries out a large amount of cut-and-fill work, from generating a large number of slope units. Due to the complexity of the slope units, if the deformation results are only decomposed into vertical and north-south directions, the horizontal deformation components outward along the aspect may be neglected, resulting in an insignificant monitoring effect. Therefore, it is necessary to consider the aspect of the terrain slope and further decompose the horizontal deformation to the characteristic direction to make the monitoring results more accurate, on the basis of the above fixed-direction two-dimensional deformation decomposition method. The horizontal deformation data of the up-orbiting satellite is further decomposed to the characteristic direction as the following equation:

$$d_{los1} = d_u \times \cos\theta_1 + d_y \times \cos(\alpha_1 - \alpha')\sin\theta_1 \tag{13}$$

In the above equation, d_u is the vertical deformation in the LOS direction projection, d_y is the eigendirection deformation in the LOS direction projection, α_1 is the angle between the flight direction of the up-orbiting satellite and the north direction, and (90°-α') is the angle between the eigendirection and the north direction. θ_1 is the radar's local incidence angle. When the LOS direction data for multiple orbits are available, the two-dimensional characteristic deformation sequence decomposition function along the horizontal aspect can be modelled:

$$Gx = d \tag{14}$$

Where $d=[(d_1\&d_2\&(\ldots\&d_N))]^T$, represents the LOS-directed deformation data of multiple tracks fused into a time-series LOS-directed deformation with N time nodes through a unified time base as shown in Fig. 1, G denotes the decomposition matrix for the decomposition of the deformations along the horizontal aspect and vertical direction, and $x=[(h_1\&u_1)\ (h_2\&u_2)\ (\ldots\&h_N\&u_N)]^T$, denoting the deformation along the horizontal slope and vertical directions for N time nodes. The orbital fusion mode is shown in figure 2.

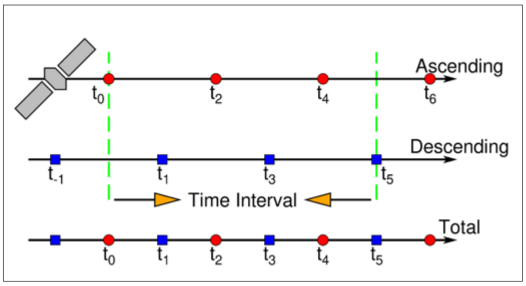

Figure 2: Schematic of Orbital Fusion

This functional model suffers from rank loss and cannot be solved for two-dimensional deformations, so constraint equations need to be introduced. The solution of the general pathological equations can be solved using Tikhonov regularization. The second order Tikhonov regularization constraint is generally chosen. The following regularized least squares solution criterion is established:

$$min\left\|\begin{bmatrix} G \\ \alpha R \end{bmatrix} x - \begin{bmatrix} d \\ 0 \end{bmatrix}\right\|_2^2 \tag{15}$$

Finally, it is solved by iterative weighted least squares until the sum of squares of the residuals of the two previous and two previous times meets the given accuracy requirements.

$$x = (G^T G + \alpha^2 (R^T R))^{-1} G^T d \tag{16}$$

This method decomposes the LOS direction deformation results obtained from InSAR data into vertical direction deformation and characteristic direction deformation by using lift track data. In this paper, in the deformation monitoring of mountain airports, the aspect can be calculated based on high-precision DEM, and the outward direction of the aspect can be designated as the eigendirection and subsequently solved.

Experiment and Results

Study Area

Weining Caohai Airport is located in the town of Caohai, Weining County, Guizhou Province, China, in the karst mountainous region of northwest Guizhou, which is under the jurisdiction of Bijie City, Guizhou Province. The geographical coordinates of the airport are roughly 26°50‘N and 104°25’E. The airport is located in the subtropical monsoon humid climate of Weining County, Guizhou Province. The airport is situated in Weining County, which experiences a humid subtropical monsoon climate with an average yearly temperature of 11.1°C. Rainfall varies significantly between years, with an average of 903.5 mm each year. 70% of the yearly rainfall occurs during the water-rich months of May through September [18]. The Weining Caohai area is dominated by limestone, which has formed a typical karst landscape through water erosion and dissolution. The area is about 2000 meters above sea level, with an alternating hilly and plateau topography, overall flat but with local hills and low-lying areas. Weining

Caohai Airport is an important civil airport in Guizhou Province and Southwest China, with a flight class of 4C and a 3,000-metre-long, 45-metre-wide international standard run. The airport is equipped with a modern terminal building (4,000 square meters) and facilities for air traffic control and firefighting, and is capable of carrying 350,000 passengers and 1,050 tons of cargo and mail throughput. Due to the complex terrain, the construction process involved extensive cut-and-fill and foundation reinforcement treatments, which successfully avoided groundwater surges and structural instability problems, ensuring the stability of the airport's foundation. The construction of this airport involves the study of complex geological conditions such as karst topography and karst geology, and is a typical case of studying airport construction and infrastructure engineering in karst topographic areas. It can provide valuable experience and technical support for highland airport construction projects under similar geological conditions. The optical image schematic diagram of Weining Caohai Airport is shown in figure 3.

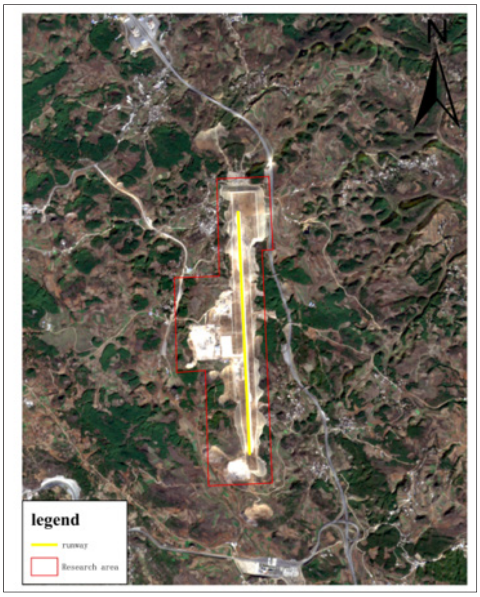

Figure 3: Schematic Optical Image of the Study Area

Data Used

The study uses data from the domestically produced Land Probe 1 SAR satellite and ESA Sentinel free data, including LT-1A SAR image data and sentinel-2 optical image data, which are used for time-series deformation resolution in the study area and optical image data are used to assist in observing the construction changes in the study area. In order to reduce the influence of signal incoherence and improve the accuracy of InSAR deformation resolution, LT-1 up-orbit image 19 and down-orbit image 20, which cover the study area and have a concentrated spatial baseline distribution in 2023-2025, are selected for the study. Meanwhile, 90 views of Sentinel-2 images covering the study area in 2018-2024 with better observation quality were selected for supporting the study. The study also used NASA SRTM DEM data with a spatial resolution of 30 m for interferogram topographic phase removal in time-series InSAR deformation resolution and for geocoding. Figure 4 shows the SAR image coverage of the study area, Table 1 shows the detailed parameters of the SAR image data, and Table 2 shows the detailed parameters of the optical image data.

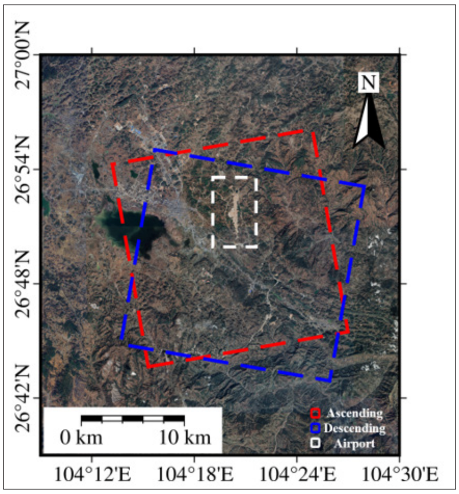

Figure 4: SAR Image Coverage of the Study Area

Table 1: Detailed Parameters of SAR Image Data

SAR Image Data	LT-1 Ascending	LT-1 Descending
Polarization mode	HH	HH
Heading angle (°)	-12.08	192.08
Incidence angle (°)	42.46	42.83
Azimuth resolution	1.73	1.73
Distance Resolution	1.67	1.66
Waveband	L	L
Number of images	19	20
Time interval	2023-07-12~2025-03-23	2023-09-10~2025-03-23

Table 2: Detailed Parameters of Optical Image Data

Optical Image Data	Sentinel-2 Data
Resolution	10m, 20m, 60m
Band	Multi-spectral instrument (MSI) covering 13 spectral bands
Number of images	90
Time interval	2018-01-17~2024-12-16

Results of Experimental Data Processing

The construction of the Weining Caohai Airport's major portion was essentially finished in 2023, according to the Sentinel-2 optical image data displayed in Figure 5. However, post-construction deformation monitoring is still required in the study region. The results of post-construction deformation monitoring in the direction of orbit upgrading and downgrading of Weining Caohai Airport after 2023 are obtained in this paper by refining the InSAR technique to process the LT-1 SAR satellite image data of orbit upgrading and downgrading from 2023 to 2025. The average deformation rate in the ascending and descending orbits is displayed in Figures 6 and 7.

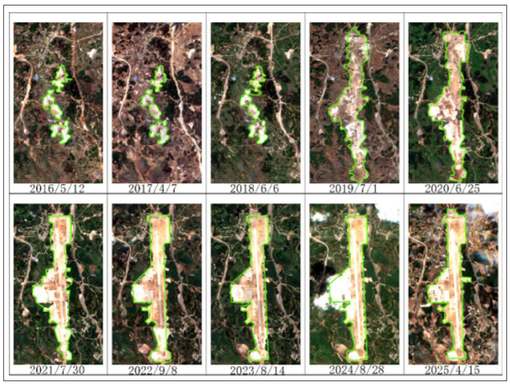

Figure 5: Optical Image Time Series

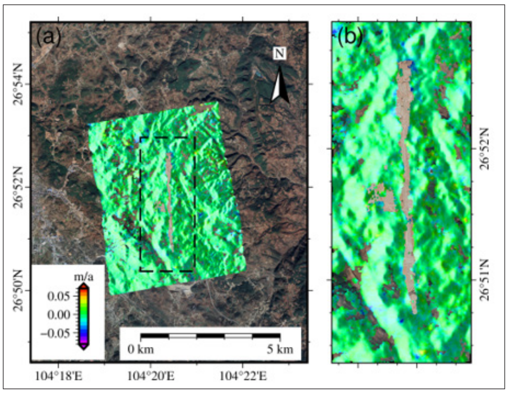

Figure 6: (a) Average Deformation Rate Results for Ascending (b) Local Deformation Rate at the Airport

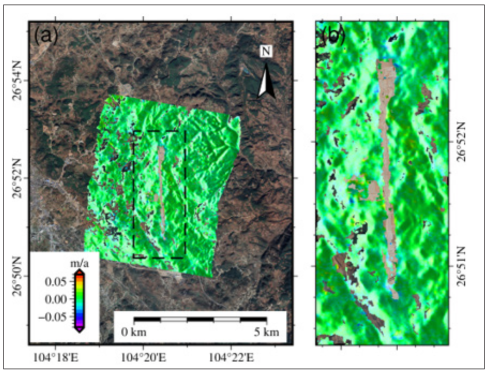

Figure 7: (a) Average Deformation Rate Results for Descending (b) Local Deformation Rate at the Airport

When the LOS directional deformation is unable to accurately depict the actual surface deformation, we employ the two-dimensional deformation decomposition method described in Chapter 2 to separate the surface deformation into east-west and vertical directions and determine the average deformation rate in each direction, as illustrated in Figure 8.

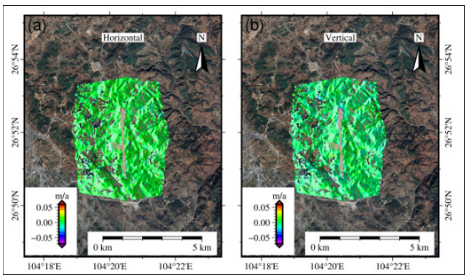

Figure 8: Two-Dimensional Characteristic Deformation Decomposition Results (a) Deformation of Horizontal Average Rate (b) Deformation of Vertical Average Rate

Discussion and Analysis

Analysis of Deformation Results

The deformation data provided detailed deformation information for many parts of the airport, such as the runway, apron, hangar, etc. Large-scale dredging and filling operations are required for the building of Weining Caohai Airport, which is situated in an area with complicated topography. The monitoring results show different levels of displacement and settlement phenomena in different areas of the airport, as shown in the following. Figure 9 illustrates the precise locations of feature points P1 and P2 at the airport. We analyze the deformation by region and choose two feature points, P1 and P2, for additional analysis. P1 is situated on the east side of the runway's north end, while P2 is situated on the west side of the runway's south end.

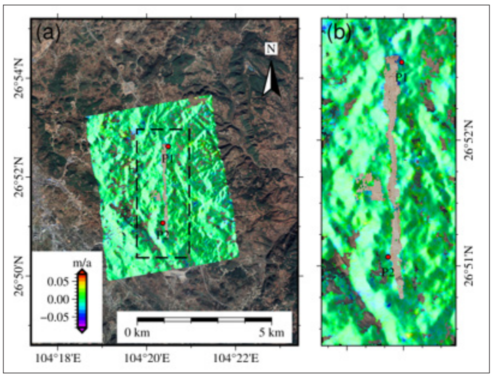

Figure 9: Position of Feature Points P1 and P2

Runway area: The airport's runway is roughly north-south and has an azimuth of 177°. Both sides of the runway displayed localized settlement, according to the data obtained. The average deformation rate of the descending track revealed that the east side of the north end of the runway exhibited a clear settlement phenomenon, with a maximum settlement rate of roughly 54 mm/year. The settlement area is primarily concentrated in the east side of the north end of the runway tail downturn platform protection area. The east side of the south end of the runway exhibited notable settlement, with a maximum settlement rate of roughly 41 mm/year, according to the lifting track's average deformation rate. With a maximum lift rate of about 33 mm/year, the east side of the runway in the midsection near the contact road displayed a notable lift. The combined lifting track data results indicate that there are isolated regions of uplift and varying degrees of settlement on both sides of the runway slope. The runway's settlement trend has certain linear features, suggesting that the uneven foundation compaction during airport building may be connected to the deformation in this location. Figure 10 shows the deformation of P1 point from the viewpoint of ascending and descending orbits while examining the deformation time series of P1 on the east side of the northern end of the runway.

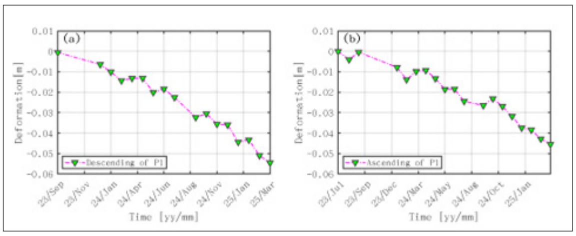

Figure 10: (a) The Time Series Deformation of the Descending Orbit at Point P1 (b) The Time Series Deformation of the Ascending Orbit at Point P1

Citation: Jun Lu, Dao Qin Zhou, Bing Xu, Jie Li, Kexin Chen, et al. (2025) Deformation Monitoring and Analysis of Mountainous Cut and Fill Airport Construction Considering Topographic and Geomorphological Features: A Case Study of Weining Caohai Airport. Journal of Earth and Environmental Science Research. SRC/JEESR-356. DOI: doi.org/10.47363/JEESR/2025(7)269

Similarly, Figure 11 illustrates the deformation of P2 point from the viewpoint of ascending and descending orbits by examining the deformation time series of P2 on the west side of the apron. It is evident that the distortion is mostly concentrated on the runway's two sides.

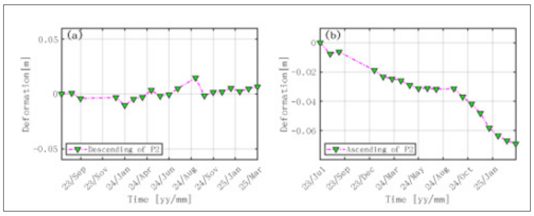

Figure 11: (a) The Time Series Deformation of the Descending Orbit at Point P2 (b) The Time Series Deformation of the Ascending Orbit at Point P2

Apron area: Settlement takes place in the vicinity of the apron, with a tiny portion of the peripheral area exhibiting a modest uplift and more noticeable settlement on the west side at a pace of roughly 36 mm/year. Bulging can occur at a maximum pace of roughly 25 mm per year. The filling operations beneath the apron, particularly in the region where the filling thickness is high, may be connected to this uneven deformation.

Terminal building foundation area: Although there is not much deformation in this area, there is still some settlement, with a maximum settlement rate of roughly 18 mm/year. Additionally, a few ancillary structures near the airport exhibit varying degrees of deformation, which could be connected to the airport's overall engineering development and operation activities.

Overall, we discovered that the ascending and descending orbit data have good spatial consistency. However, because the ascending and descending orbits have different incidence angles and flight azimuths, their maximum deformation rates differ, and the phenomenon of the opposite direction of deformation occurs in local areas. Therefore, we use the two-dimensional characteristic deformation decomposition approach to break down the LOS deformation into vertical and east-west deformation in order to better expose the spatial distribution characteristics of the post-work deformation at Caohai Airport.

At the airport, vertical deformation shows areas of uplift or settlement. Three clear deformations can be seen by observation. First, there is a clear uplift phenomenon on the west side of the runway's south end, with a maximum vertical uplift rate of 40 mm per year. The second is the east side of the north end of the runway tail decline platform protection area. The ascending and descending track LOS deformation statistics are in line with the more noticeable settlement, with a maximum settlement rate of 68 mm per year. The terminal building foundation area, which has a maximum lift of 22 mm/year, is the third location.

The local horizontal deformation can be observed with the help of east-west deformation. In total, there are two clear deformations. The first is that there is noticeable horizontal deformation on the west side slope of the runway's south end. The deformation is extruding to the runway and oriented west, with a maximum deformation rate of 55 mm/year. Second, there was localized distortion in the airport terminal building's foundation region, with a maximum deformation rate of 82 mm/year heading eastward and a maximum deformation rate of 88 mm/year going westward. After two-dimensional deformation, Figure 12 depicts the east-west and vertical deformation of point P1. It is clear that there is settlement at this location, with a maximum settlement of 68 mm but virtually no horizontal displacement. Following two-dimensional deformation decomposition, Figure 13 displays the P2 point's vertical deformation and east-west deformation. It is evident that the point has substantial sinking, with a maximum subsidence of 42 mm and a maximum horizontal displacement of 55 mm toward the west.

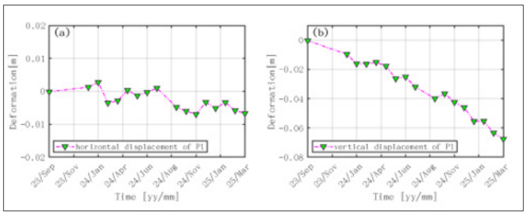

Figure 12: (a) Horizontal Deformation of Point P1 (b) Vertical Deformation of Point P1

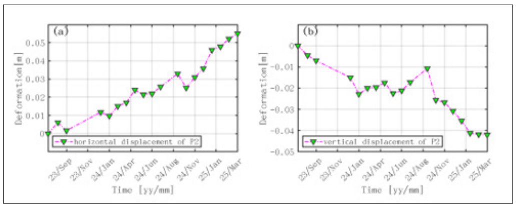

Figure 13: (a) Horizontal Deformation of Point P2 (b) Vertical Deformation of Point P2

The findings also indicate that the airport's deformation varies somewhat over time and space. The deformation rate in the time series was higher when the airport's construction was first finished and progressively stabilized over time. In the area of the construction cut-and-fill activities, the deformation is mostly concentrated in the airfield's core and periphery areas, with very little deformation in the central area.

Analysis of Deformation Drivers

Geological conditions, construction techniques (fill and cut works), groundwater seepage characteristics, and airport operations all have an impact on Weining Caohai Airport's post-construction deformation. The driving factors of the two more noticeable post-production deformations (the eastern slope at the northern end of the runway and the western slope at the southern end of the runway) in the monitoring results are thoroughly examined in this paper, taking into consideration the actual geological conditions as well as the features of the filling and excavation operations at the Weining Caohai Airport.

The area of the eastern slope at the northern end of the runway: abnormal uplift has occurred in this area, which may be related to the physical-mechanical properties of the foundation soils, which are uneven in the complex geological conditions of the area where the airport is located. In some areas, there may be weak soil layers or insufficient compaction of the fill, leading to uneven settlement of the airport facilities during construction.

Uneven distribution of soil layers: The runway slopes of the airports are all subject to some degree of settlement, which may be due to the fact that the soft soil layers in some areas of the airports are subject to consolidation and settlement under loading, while the insufficient compaction of the fill areas may lead to localized settlement. This inhomogeneity is one of the main driving factors for the occurrence of uneven settlement on runway slopes.

Soil consolidation characteristics: some consolidation settlement may occur during compaction of the soil in the fill area, and if the fill load is not adequately compacted, it may rebound after consolidation settlement at a later stage; the use of lightweight materials (e.g., foam concrete) may also lead to localized bulging. The anomalous uplift of the eastern slope at the southern end of the runway may be related to insufficient compaction of the fill load in the fill area.

The area of the western slope at the northern end of the runway:uneven deformations have been observed in this area, with both settlement and uplift phenomena. These phenomena may be related to the fact that the foundation construction process involved a large number of filling and excavation works, and that these activities had a significant impact on the stability of the airport. Soils in the fill areas may undergo consolidation and settlement during compaction, while localized uplift may occur in the excavated areas as a result of soil unloading.

Filled Areas
Soils in filled areas may undergo consolidation settlement during compaction, especially in areas where the fill thickness is large. For example, the settlement in part of the apron may be related to the consolidation of soil in the fill area.

Excavated Areas
Localized uplift of soil in excavated areas may occur as a result of unloading. For example, the deformation of the airport edge area may be related to the unloading of soil in the excavated area.

Uneven Settlement
Unevenness of fill and excavation works leads to differences in settlement rates in different areas of the airport, and such differences may be an important driver of the deformation of the airport terminal building foundations.

Underground engineering impacts: improper pressure control during grouting to reinforce the foundations may lead to soil expansion. Pipeline excavation underneath the terminal building, underground car parks and other works may change the soil stress and trigger ground uplift in the surrounding area.

Conclusion
This study uses Sentinel-2 optical pictures and domestic Land Tracking-1 (LT-1) SAR satellite data, based on the enhanced time-series InSAR technique, to monitor and analyze the post-work deformation of the Caohai Airport in Weining, Guizhou Province, with high precision. Aiming at the complex terrain and geomorphological features of mountain airports, the study proposes a homogeneous point identification optimization method that takes into account slope, slope direction and feature cover type, and constructs a 2D feature deformation decomposition model by combining the lifting and lowering orbit data, which realizes the accurate solution of deformation in the vertical and horizontal feature directions. The following are the primary findings of the study:

- **Deformation Monitoring Technique Optimization:** By adding the weighting component of terrain features to the homogeneous point identification method of DS-InSAR, the monitoring accuracy in difficult terrain conditions is greatly increased. In the meantime, a more thorough deformation field analysis is obtained by successfully overcoming the geometric constraint of single-track monitoring through the fusing of lift track data.
- **Post-Construction Deformation Characteristics:** The runway, apron, and terminal areas exhibit different levels of heave and settlement, according to monitoring data. While the local settlement rate on the west side of the southern end of the runway is 42 mm/year, with a horizontal deformation rate as high as 55 mm/year, the greatest settlement rate on the east side of the northern end is 68 mm/year. There is still a chance that small areas will continue to deform, even if time series analysis shows that the rate of deformation was higher in the early phases of construction and steadily stabilized later.
- **Analysis of Deformation Causes:** When combined with the engineering geological conditions, it was found that the primary causes of uneven deformation were uneven compaction of the fill, consolidation of weak soil layers, and disturbance of underground works. This provided a scientific foundation for the airport's subsequent maintenance, and the InSAR technique assisted in evaluating the effects of the settlement of the airport construction and its surrounding infrastructures on the geological environment, including the possible effects on the nearby roads, buildings, and groundwater system. effects. Airport authorities can take prompt action to avoid excessive settlement from endangering airport operations' safety thanks to this assessment.

References

1. Dai K, Shi X, Gou J, Hu L, Chen M, et al. (2020) Diagnosing Subsidence Geohazard at Beijing Capital International Airport, from High-Resolution SAR Interferometry. Sustainability 12: 2269.
2. Jiang Y, Liao M, Wang H, Zhang L, Balz T (2016) Deformation Monitoring and Analysis of the Geological Environment of Pudong International Airport with Persistent Scatterer SAR Interferometry. Remote Sens 8: 1021.
3. Songbo Wu, Zefa Yang, Xiaoli Ding, Bochen Zhang, Lei Zhang, et al. (2020) Two decades of settlement of Hong Kong International Airport measured with multi-temporal InSAR. Remote Sensing of Environment 248: 0034-4257.
4. Daozhen Pang (2016) High-fill foundation treatment technology under complex geological conditions in Jiuzhai Huanglong Airport. J Building construction 38: 679-681.
5. Yang Chen, Gang Du, Fenfei Gao (2011) Numerical simulation of deformation and stability of high fill foundations at Kangding Airport [J]. Roadbed Engineering 2: 111-114.
6. Guoquan Lai, Haiping Jiao, Honggang Wu (2025) Characteristics of high-fill landslides in mountainous airports, disaster mechanisms, prevention and control, and revelations: a case study of Panzhihua Airport [J]. Geoscience Bulletin 1-14.
7. Xuemei Gao (2008) Study on foundation stability of high fill body at the northeast end of Liupanshui Airport, Guizhou Province [D]. Chengdu University of Technology.
8. Ferretti A, Fumagalli A, Novali F, Claudio Prati, Fabio Rocca, et al. (2011) A New Algorithm for Processing Interferometric Data-Stacks: SqueeSAR [J]. IEEE Transactions on Geoscience & Remote Sensing 49: 3460-3470.
9. Hooper, Andrew (2008) A multi-temporal InSAR method incorporating both persistent scatterer and small baseline approaches [J]. Geophysical Research Letters 35: 96-106.
10. Michel R, Avouac J P, Taboury J (1999) Measuring ground displacements from SAR amplitude images: Application to the Landers earthquake [J]. Geophysical Research Letters 26: 875-878.
11. Bechor NBD, Zebker HA (2006) Measuring two-dimensional movements using a single InSAR pair [J]. Geophysical

Research Letters 33: 275-303.
12. Ferretti C Prati, Rocca F (2001) Permanent scatterers in SAR interferometry. IEEE Transactions on Geoscience and Remote Sensing 39: 8-20.
13. Berardino P, Fornaro G, Lanari R, Sansosti E (2001) A new algorithm for surface deformation monitoring based on small baseline differential SAR interferograms. IEEE Transactions on Geoscience and Remote Sensing 40: 2375-2383.
14. Yibin Wu, Hongbin Ge, Guangqing Liu (2021) Settlement monitoring of Xiamen new airport reclamation area based on MT-InSAR technology [J]. Engineering Exploration 49: 57-61.
15. Huihui Mei, Jingchun Zhou, Yong Liu (2024) Study on runway deformation monitoring of Yunnan Wenshan Yanshan Airport based on time series InSAR technology [J]. Surveying and Mapping Bulletin S2: 211-216.
16. Xianbin Luo (2024) Research on settlement monitoring and prediction of reclaimed airports based on time series InSAR and long and short-term memory network [D]. Jiangxi University of Technology.
17. Gagliardi V, Bianchini Ciampoli L, Trevisani S, D'Amico F, Alani AM, et al. (2021) Testing Sentinel-1 SAR Interferometry Data for Airport Runway Monitoring: A Geostatistical Analysis. Sensors 21: 5769.
18. Pei Liu (2014) Research on karst hydrogeological conditions and karst water resources evaluation in Caohai area, Weining, Guizhou [D]. Chengdu University of Technology, China.